ECS Journal of Solid State Science and Technology, **2** (9) P346-P350 (2013)
2162-8769/2013/2(9)/P346/5/$31.00 © The Electrochemical Society

Implantation and Activation of Phosphorus in Amorphous and Crystalline Germanium Layers

R. R. Lieten,[a,b,c,z] B. Douhard,[c] A. Stesmans,[a,*] M. Jivanescu,[a] J. W. Beeman,[b] E. Simoen,[c,*] W. Vandervorst,[a,c] E. E. Haller,[b,d] and J.-P. Locquet[a]

[a]*Department of Physics and Astronomy, KU Leuven, Belgium*
[b]*Materials Sciences Division, Lawrence Berkeley National Laboratory, Berkeley, California 94704, USA*
[c]*IMEC, 3001 Leuven, Belgium*
[d]*Department of Materials Science and Engineering, University of California, Berkeley, Berkeley, California 94704, USA*

We have investigated phosphorus implantation and activation in amorphous and crystalline Ge layers, deposited on Si substrates. The structure of the Ge layer has only limited influence on the dopant profile and diffusion after annealing. Surprisingly, crystalline Ge layers show better electrical results after implantation and dopant activation. For the amorphous layer, the solid phase epitaxy process is influenced in the neighborhood of P, leading to point defects, which inhibit electrical activation. This result implies that when a crystalline Ge layer is amorphized during implantation of high doses, the dopant activation can be significantly reduced. Reduced temperature ramping improves activation of P in amorphous Ge layers.
 [DOI: 10.1149/2.011309jss]

Manuscript submitted April 19, 2013; revised manuscript received June 7, 2013. Published June 18, 2013.

Germanium shows interesting electrical and optical properties, including high carrier mobilities[1] and large optical absorbance[2] compared to silicon. The high electron and hole mobilities make Ge suitable as channel material for future nanoscale CMOS devices. Doping of Ge layer can be achieved by introducing dopants during deposition (co-deposition) or by implantation after deposition. The disadvantage of implantation is the introduction of structural defects:[3] vacancies and interstitials. Structural defects can lead to dopant loss during thermal annealing,[4] cause enhanced scattering of carrier leading to lower carrier mobilities, and compensate n-type doping. In addition, excess point defects introduced during ion implantation can lead to transient enhanced diffusion, well known for the case of B in Si.[5,6] To circumvent the introduction of structural defects during implantation of dopants, we have fabricated amorphous Ge layers on Si. After implantation, the a-Ge layers were annealed to achieve solid phase epitaxy (SPE). SPE of Ge on Si can be achieved at relatively low temperatures of 400°C and transforms an amorphous Ge layer into a single crystalline Ge layer on Si.[7] In this work we investigate the influence of the structure (amorphous, crystalline) of Ge on the implantation and activation of phosphorus. P seems to be the most suitable donor as it allows the highest activation level and has a lower diffusivity in Ge than As and Sb.[8]

Experimental

Amorphous (a-Ge) and crystalline Ge (c-Ge) layers have been deposited by molecular beam deposition (MBE) and plasma enhanced chemical vapor deposition (PECVD) on Si(111) substrates. Prior to deposition the Si substrates were chemically cleaned to remove metal contamination, particles, and native oxide. Immediately thereafter the samples were loaded into the deposition system. The Ge layers have a thickness of about 100 nm and 150 nm for MBE and PECVD, respectively. Implantation of P has been performed with a dose, energy and tilt of 1.0×10^{14} cm^{-2}, 50 keV, and 7°, respectively. For a corresponding implantation depth of 100 nm, these implantation conditions introduce a P concentration of about 1.0×10^{19} cm^{-3} as calculated with SRIM.[9] This is below the active P concentration limit of 2×10^{19} cm^{-3} for the occurrence of concentration-enhanced diffusion, leading to box-shaped profiles.[11] In this case, diffusion is dominated by the intrinsic P-diffusion and the focus can be on the maximum active concentration or activation degree, which can be reached in amorphous and crystalline germanium. Additionally to P implantation of a-Ge and c-Ge we have fabricated a-Ge layers with co-doping of P, and crystallized this layer by SPE. X-ray diffraction (XRD) has been performed for structural analysis. Secondary ion mass spectrometry (SIMS) is used to analyze the doping profile and diffusion of P. Hall effect measurements are used to assess the resistivity, carrier concentration and mobility.

Results and Discussion

The influence of the Ge structure on P implantation and activation has been investigated using a-Ge and c-Ge layers. A c-Ge layer has been obtained by epitaxial growth on a p-type Si(111) substrate at 450°C (sample 1) in the MBE system. A reduction in adatom surface mobility is required to achieve an a-Ge layer (sample 2) on a crystalline Si(111) substrate.[7] This has been achieved by exposing the surface to an inert N_2 beam during deposition in the MBE system and lowering of substrate temperature to around 50°C. A Ge deposition rate of 120 nm/h was used for all experiments, corresponding to a beam equivalent pressure of 1.4×10^{-7} Torr ($\sim 10^{14}$ Ge atoms/cm^2 s). A beam of molecular nitrogen (N_2) was added during deposition with a beam equivalent pressure of around 1×10^{-5} Torr. Reflection high energy electron diffraction (RHEED) confirms that the layer is amorphous. The crystalline (sample 1) and amorphous (sample 2) Ge layers received P implantation of 1.0×10^{14} cm^{-2} dose. After implantation the samples are annealed in N_2 ambient for 1 minute with a ramp rate of 15°C/s. This annealing step initiates solid phase epitaxy for the amorphous Ge samples[7] and recrystallization for the epitaxial layers.[10] Hall effect measurements have been performed of which the results are summarized in Table I. The epitaxial Ge layer (sample 1a: c-Ge, P implanted, 700°C annealed) shows excellent activation of P doping: resistivity, electron concentration, and mobility of 3.2×10^{-3} Ohm.cm, 5.7×10^{18} cm^{-3} and 347 cm^2/V s respectively. The amorphous layer, however, did not show n-type conductivity after implantation and SPE (sample 2a: a-Ge, P implanted, 700°C annealed). The p-type conductivity that was measured for sample 2a, follows from the p-type conductivity of the Si substrate. The structure of the Ge layer has therefore a significant influence on the activation of P. The difference in activation results between epitaxial Ge and amorphous may have several reasons: (1) deeper implantation for amorphous layers, (2) increased diffusion of P in amorphous layers, (3) higher impurity concentrations which compensate P doping, (4) nucleation by implantation leading to poly crystalline SPE, (5) reduced structural quality which leads to compensation of P doping or reduced carrier mobility, (6) nucleation by the presence of P or implanted impurities which leads to poly SPE, (7) formation of neutral complexes of P and defects, which inhibit electrical activation of P. In the following sections we investigate these possible causes in more detail.

*Electrochemical Society Active Member.
[z]E-mail: ruben.lieten@gmail.com

Table I. Hall effect results of implanted amorphous and crystalline Ge after annealing (samples 1, 2 and 3) and P doped a-Ge after annealing (sample 4).

Sample	Structure after deposition	Pre-annealing (°C)	Post-annealing (°C)	Resistivity (Ohm.cm)	Carrier type	Carrier conc. (cm^{-3})	Mobility ($cm^2/V\ s$)
Sample 1a	crystalline	/	700	3.2×10^{-3}	n	5.7×10^{18}	347
Sample 1b	crystalline	/	600	3.8×10^{-3}	n	7.8×10^{18}	208
Sample 2a	amorphous	/	700	2.9×10^{-2}	p	3.1×10^{18}	69
Sample 2b	amorphous	/	600	3.3×10^{-2}	p	3.4×10^{18}	56
Sample 2c	amorphous	600	600	4.5×10^{-1}	n	7.6×10^{17}	288
Sample 3a	amorphous + H	/	700	4.0×10^{-2}	p	2.7×10^{18}	58
Sample 3b	amorphous + H	/	450, slow	2.5×10^{-1}	n	1.2×10^{17}	211
Sample 4	amorphous + H + P codoped	/	600	9.0×10^{-3}	n	2.6×10^{18}	271

(1) First we investigate if there is a difference in implantation profile. The implantation profile of P in a-Ge and c-Ge has been investigated by SIMS measurements, see Figure 1. The integrated P content is 1.4 times higher for the c-Ge. This difference is most likely due to the difference in matrix structure and a difference in oxygen concentration, which influences the SIMS measurements.

(2) Next we look at the possibility of enhanced P outdiffusion in a-Ge compared to c-Ge. Diffusion of P in Ge is vacancy-assisted and therefore highly dependent on the presence of vacancies.[11] Therefore it is expected that diffusion of P during thermal annealing will be different for amorphous and crystalline layers. SIMS measurements have been performed to investigate the diffusion of P in amorphous and crystalline Ge during thermal annealing, see Figure 1. The integrated P content decreases 7% for the P implanted c-Ge sample after annealing at 700°C (sample 1 a) compared to before annealing (sample 1d). For the P implanted a-Ge sample, the integrated P content decreases with 26% after annealing at 700°C (sample 2a) compared to before annealing (sample 2e). For the a-Ge (sample 2) the measurement of P content will be influenced by the difference in matrix structure and a difference in oxygen concentration. However it is clear that P diffusion cannot be responsible for the significant difference in P activation between c-Ge (sample 1) and a-Ge (sample 2). Solid phase epitaxy of amorphous Ge occurs around 400°C.[7] Our results show that significant P diffusion in the amorphous Ge matrix does not occur before SPE. After crystallization the diffusion in both samples does not differ significantly. Similar results were obtained for P implanted Ge layers that were amorphized by Ge implantation and which did not show significant influence of implantation defects on the diffusion coefficient.[12] We observe a steeper drop in P concentration for the amorphous Ge, see Figure 1. Much less (<1%) Si diffusion into the Ge layer, is observed for the amorphous Ge (not shown), which follows from the much lower deposition temperature (50°C compared to 450°C). When the P solubility limit is exceeded (2×10^{20} cm^{-3} at 600°C) dopant precipitation into inactive precipitates will occur[13] which can be observed by SIMS as a dopant concentration "spike".[14] In our experiments we obtained P concentrations of 1×10^{19} cm^{-3} and did not observe dopant concentration "spikes" within the Ge layer. At the Ge-Si interface, segregation of P is observed for both samples, however 10 x more for the crystalline sample. At the surface also a P peak in concentration is measured.

(3) Additionally, we investigate the influence of impurity concentrations on P activation in a-Ge and c-Ge. The presence of impurities can induce additional carriers in the layer or reduce the carrier mobility. An example is hydrogen, which can passivate P by forming inactive P-H complexes.[15] However in case such complexes would be present in our samples, P-H bonds would dissociate during the activation annealing. SIMS measurements indicate the presence of much more O in the amorphous Ge (1000 times) than in the crystalline Ge (not shown) after deposition. This can be explained by an increase in oxygen and humidity absorption at low deposition temperatures and higher background pressure. After annealing the O content in the crystalline layers increases near the surface and the difference in O concentration decreases significantly: the O concentration is 7 times higher for the annealed amorphous layer than for the annealed crystalline sample. The normal lattice site for oxygen in Ge is interstitial and is electrically inactive.[16] The higher O concentration in the amorphous layers can lead to lower mobility values. Furthermore O can cause passivation of P. However these effects cannot explain the large difference in activation of P in the amorphous and crystalline Ge layers. Please note that the high amount of O present in the a-Ge influences secondary ion yields during SIMS measurements. P profiles on Figure 1 have therefore been corrected to take that matrix effect into account using point-by-point data correction with respect to matrix signal but some artificial variations are still influencing slightly the plotted profile shape.

(4) Subsequently, we look at the possibility of crystallite nucleation by implantation in a-Ge. P ions lose gradually their energy by collisions with nuclei and can therefore introduce structural reordering of the host matrix. Implantation of P can therefore induce the formation of crystalline nuclei in the amorphous matrix. Crystalline nuclei will lead to polycrystalline Ge upon crystallization.[17] The presence of poly crystalline grains has been

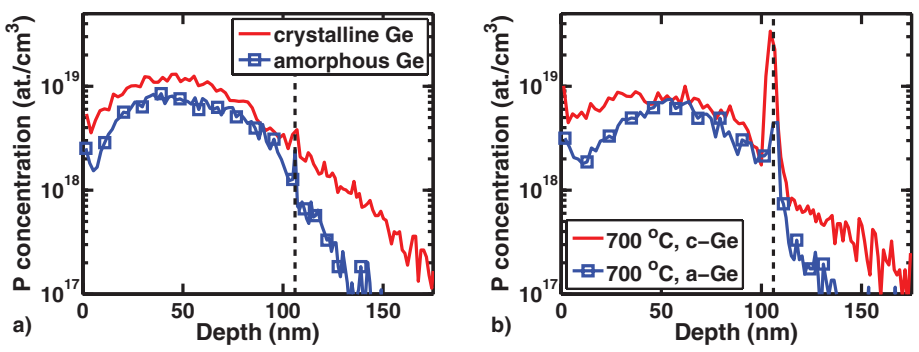

Figure 1. a) Point-by-point corrected phosphorus profile, measured by SIMS, in crystalline (sample 1d) and amorphous Ge (sample 2e) before annealing. b) Phosphorus profile in crystalline (sample 1a) and amorphous Ge (sample 2a) after annealing. The dashed lines indicate the Ge/Si interface.

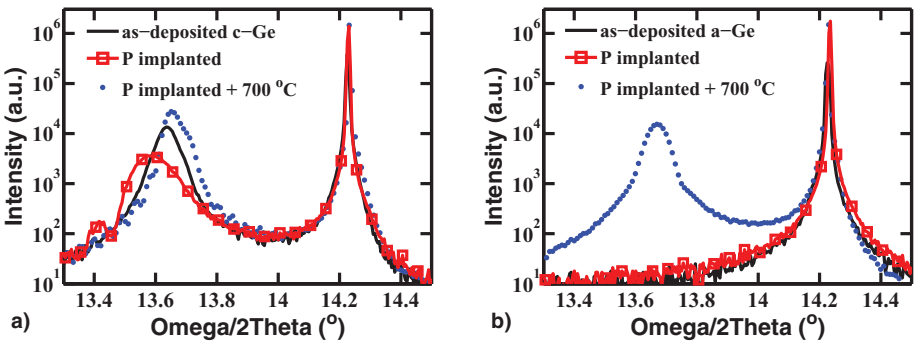

Figure 2. a) XRD ω/2θ scan of epitaxial Ge (sample 1e, black, solid line), implanted epitaxial Ge (sample 1d, red, solid line with squares) and implanted epitaxial Ge after annealing at 700°C (sample 1a, blue, dotted lined). b) XRD ω/2θ scan of amorphous Ge (sample 2d, black, solid line), implanted amorphous Ge (sample 2e, red, solid line with squares) and implanted amorphous Ge after annealing at 700°C (sample 2a, blue, dotted lined).

investigated by grazing incidence XRD 2θ scans (not shown). No diffraction peaks were observed for the as deposited a-Ge layer (sample 2d) and implanted a-Ge sample (sample 2c), indicating there are no poly crystalline grains present in the layers before and after implantation.

(5) Furthermore we investigate the possibility of a difference in defect concentrations between the implanted and activated a-Ge and c-Ge layers. Vacancies in Ge are acceptors,[18] which can compensate P doping. Therefore it is important to achieve Ge layers with low vacancy densities. SPE of a-Ge deposited by PECVD and co-doped with P (sample 4) shows excellent activation: for 90 nm we obtained an electron concentration, mobility and resistivity of 2.6×10^{18} cm^{-3}, 271 cm^2/V s and 0.009 Ohm.cm, respectively,[11] see Table I. This shows that the structural quality of crystalline Ge formed by SPE is excellent and leads to good electrical results. The influence of implantation on the structure of amorphous and crystalline Ge layers has been investigated by XRD measurements. Without implantation, the epitaxially grown c-Ge layer (sample 1c) and the crystallized a-Ge layer (sample 2f) show comparable crystal quality, see Figure 2. The XRD full width at half maximum (FWHM) of the (111) reflection is comparable for the epitaxial and SPE sample, see Table II. The P implantation leads to strain in the Ge layer (sample 1d): the a spacing decreases and the c spacing increases with a strain of +0.4%. After annealing, the strain for the c-Ge (sample 1a: P-implanted, 700°C annealed) is reduced to 0.0%. For the a-Ge sample the layer becomes tensile strained: the a-spacing increases and the c spacing decreases with a strain of −0.16% for sample 2a (a-Ge, P implanted, 700°C annealed) and −0.19% for sample 2f (a-Ge, no implantation, 600°C annealed). This tensile strain follows from the thermal mismatch of Ge and Si at the annealing temperatures. Although the crystal quality as assessed by XRD seems comparable there can be significant differences in point defect densities. This will be addressed later in section (7).

(6) Subsequently we investigate the influence of implanted P atoms on the nucleation during the crystallization process of a-Ge. To investigate the influence of implanted P on the nucleation, we compare the structural quality of the amorphous sample with and without implantation followed by SPE (sample2a: a-Ge, P implanted, 700°C annealing and sample 2f: a-Ge, 600°C annealing, respectively). The XRD FWHM values of the (111) reflection show comparable structural quality, see Table II. Grazing incidence XRD 2θ scans (not shown) did not show diffraction peaks for the implanted amorphous layer after SPE, indicating that the presence of implanted P does not lead to nucleation of random grains.

(7) Finally, we look at the formation of neutral complexes of P and defects. The influence of P on the solid phase epitaxy process can be assessed by comparing the activation of implanted P in an amorphous layer (sample 2b: a-Ge, P implantation, 600°C annealing) and an amorphous layer, first crystallized before P implantation (sample 2c: a-Ge, 600°C pre-annealing, P implantation, 600°C post-annealing). The results are summarized in Table I. N-type conductivity was observed for the SPE sample when the implantation was performed after crystallization (sample 2c). The structure of the Ge layer before P implantation (a-Ge for sample 2b and c-Ge for sample 2c) has therefore a clear influence on the dopant activation. Previously it has been shown that the velocity of recrystallization of Si is increased for doping concentrations exceeding about 10^{20} cm^{-3}.[19] Also for Ge it has been demonstrated that dopants influence the crystallization velocity.[20,21] The SPE process is influenced by the electronic properties of the dopants as well as the introduction of local strain.[21] Our results indicate that, besides an influence on the crystallization kinetics, the solid phase crystallization process is influenced by implantation of P into an amorphous Ge layer. XRD shows a comparable structural quality, which is mainly determined by the amount of extended defects, and therefore a difference in point defects in the neighborhood seems likely. The electrical results of the amorphous sample which was first crystallized before implantation (sample 2c: a-Ge, 600°C pre-annealing, P implantation, 600°C post-annealing) shows that the structural quality of crystallized amorphous Ge and the impurity concentrations are good enough to obtain P activation. The carrier concentration of this sample is a factor 10 times lower than for the implanted crystalline sample, which can be explained by a difference in crystal quality or impurity concentration. We therefore conclude that in the case of implantation of the a-Ge (sample 2b) the crystallization process in the neighborhood of P is influenced, leading to point defects which inhibit electrical activation of P. It has been reported that P can form clusters with vacancies, which inhibits electrical activation.[22] Therefore, it seems likely that P-vacancy clusters are formed during SPE of P

Table II. Summary of structural characterization by XRD.

Sample	Structure after deposition	P implant.	Post-annealing (°C)	(111) FWHM (arc sec)	c spacing (Å)	Ec Strain (%)
Sample 1a	crystalline	yes	700	392	5.658	+0.00
Sample 1c	crystalline	/	/	356	5.659	+0.02
Sample 1d	crystalline	yes	/	244	5.682	+0.42
Sample 2a	amorphous	yes	700	212	5.649	−0.16
Sample 2d	amorphous	/	/	/	/	/
Sample 2e	amorphous	yes	/	/	/	/
Sample 2f	amorphous	/	600	223	5.647	−0.19

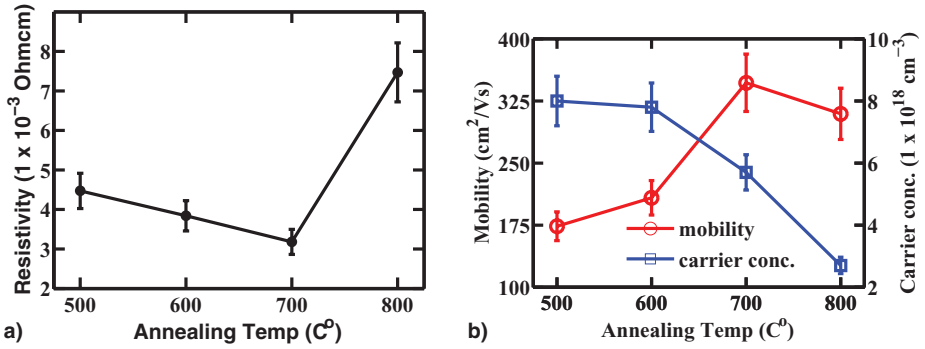

Figure 3. (a) Resistivity for implanted crystalline Ge (sample 1) at different annealing temperatures. The lowest resistivity was obtained for annealing at 700°C. **(b)** Carrier mobility and concentration at different annealing temperatures. Above 600°C P out diffusion becomes significant. The mobility increases for increasing annealing temperature till 700°C. At 800°C the mobility is reduced due to increased surface and interface roughness.

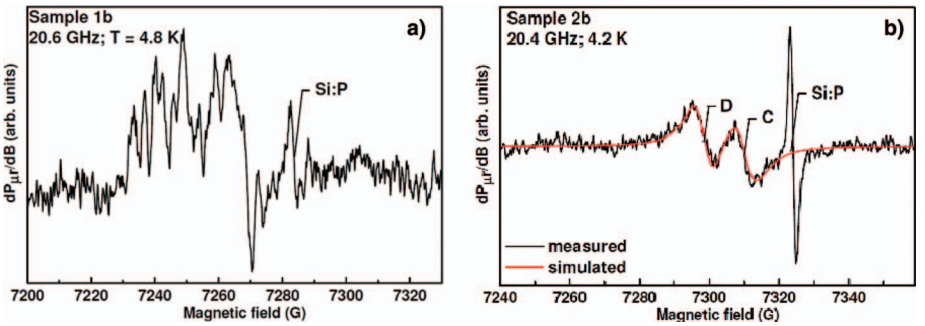

Figure 4. K-band ESR spectra observed on (a) sample 1b (epitaxial Ge layer 1, P implanted, 600°C annealed) and (b) sample 2b (amorphous Ge layer, P implanted, 600°C annealed) for comparable total sample areas, using an applied microwave power of ~25 nW and modulation field amplitude of 0.9 G. The signal labeled "Si:P" stems from a co-mounted Si:P reference sample of g (4.2 K) = 1.99869.

implanted amorphous Ge. To assess a difference in the presence and activation of point defects, we have performed electron spin resonance (ESR) measurements. ESR indeed show a significant difference in the type and density of paramagnetic defects, see Figure 4. For sample 1b (c-Ge, P implanted, 600°C annealed) ESR spectra show partly anisotropic signals arising from paramagnetic centers with a total areal density above 3×10^{13} cm^{-2}. They likely originate from defects in a crystalline layer, here the epi Ge layer. The signals, however, appear too weak to enable reliable in depth defect tracing. For sample 2b (a-Ge, P implanted, 600°C annealed) two types of defects, in significantly lower densities, are observed in the ESR spectra: D line (Si dangling bonds in an amorphous Si environment) and, likely, carbon-related defects, amounting to a density of [D] = $(4.8 \pm 0.1) \times 10^{12}$ cm^{-2} and [C] = $(5.9 \pm 0.2) \times 10^{12}$ cm^{-2}. None of the signals are angle dependent. Sample 1b showed much more microwave dissipation of the microwave power than sample 2b, which follows from the higher electrical conductivity. The difference in P activation for both samples, will lead to a difference in the position of the Fermi level. This explains why we clearly see the presence of point defects for sample 1b, although the point defect concentration for sample 2b should be much higher following the low P activation.

From the previous section it is clear that in case of implantation the crystallization process in the neighborhood of P is influenced, most likely leading to point defects which inhibit electrical activation of P. In a next step we have investigated the influence of annealing conditions on P activation in crystalline and amorphous Ge films. With the sample in N_2 ambient, the annealing temperature is ramped at 15°C/s to the maximum annealing temperature and kept for 1 min. In case of amorphous Ge, no successful n-type conductivity was observed for this RTA treatment for temperatures between 500 and 800°C. In case of P implanted c-Ge, annealed at 700°C (sample 1a) showed the lowest resistivity: 3.2×10^{-3} Ohm.cm, for an electron concentration of 5.7×10^{18} cm^{-3} and mobility of 347 cm^2/V s, see Table III and Figure 3. Annealing at 500 and 600°C shows the highest electron concentration of 8.0×10^{18} cm^{-3}. At higher temperatures the electron concentration decreases due to P out diffusion. The mobility increases for increasing temperature due to improvement in structural quality. At 800°C the mobility is slightly lower than at 700°C, which can be explained by increased surface and interface roughness. Without annealing, n-type conductivity is not observed, confirming that thermal treatment is mandatory after implantation. The mobility of 347 cm^2/V s for sample 1a (c-Ge, P implanted, 700°C annealed) is close to that of bulk Ge (410 cm^2/V s)[1]. When comparing the P profile in the implanted epitaxial sample without activation anneal (sample 1d) and the activated sample (sample 1a: c-Ge, P implanted, 700°C annealed), 7% less P is found in the annealed sample.

Finally we have investigated the influence of hydrogen and the annealing procedure on P activation. Previously it has been shown that the presence of hydrogen in a-Ge reduces the SPE growth velocity.[20] Amorphous Ge layers were deposited by PECVD, with high hydrogen concentrations (a few atomic%) and implanted with P with a dose and tilt of 1.0×10^{14} cm^{-2}, 50 keV, and 7°, respectively (sample 3). Annealing at 700°C with 15°C/s ramping did not give satisfactory P activation, see sample 3a in Table I. Slow ramping of 1.5°C/min to 450°C showed P activation (sample 3b): resistivity, electron

Table III. Electrical properties of P implanted crystalline Ge films (epitaxial sample 1) for activation annealing temperatures between 500 and 800°C.

Annealing temperature (°C)	Resistivity (Ohm.cm)	Carrier type	Carrier conc. (cm^{-3})	Mobility (cm^2/V s)
/	2.6×10^{-3}	p	7.5×10^{18}	32
500	4.5×10^{-3}	n	8.0×10^{18}	174
600	3.8×10^{-3}	n	7.8×10^{18}	208
700	3.2×10^{-3}	n	5.7×10^{18}	347
800	7.5×10^{-3}	n	2.7×10^{18}	310

concentration and mobility of 2.5×10^{-1} Ohm.cm, 1.2×10^{17} cm^{-3} and 211 cm^2/V s, respectively. The annealing procedure has therefore a large influence on the activation. When applying the same annealing procedure to the implanted amorphous Ge without hydrogen, no activation was observed, indicating that the presence of hydrogen does not only influence the velocity of the SPE process but also influences P activation. However additional H implantation after P implantation did not improve the activation further.

A conclusion from these results is that for high implantation doses, for which the layer is completely amorphized, the crystallization process in the neighborhood of P is influenced and the dopant activation efficiency decreases. Therefore it is advisable to divide a high dose into multiple lower doses and activate these doses in between to prevent complete amorphization and low activation. This concept has been recently demonstrated.[23]

Conclusions

We have investigated phosphorus doping of Ge by implantation. A disadvantage of implantation is the introduction of structural defects. To circumvent the introduction of structural defects during implantation of dopants, we start from an amorphous Ge layer. Phosphorus is implanted into the amorphous layer and solid phase epitaxy (SPE) is applied. Surprisingly starting from crystalline Ge layers gives better electrical results over a-Ge layers after implantation and annealing. In view of this difference in P activation we have investigated the crystallization behavior of P implanted a-Ge. Our results show that the structure has significant influence on the activation of implanted P. However, the structure of the a-Ge layer has only a limited influence on the dopant profile and dopant diffusion after annealing. In contrast to implantation, co-doping of P during deposition followed by SPE gives excellent electrical activation. X-ray diffraction shows comparable structural quality for samples with and without P implantation after SPE. We conclude that in case of implantation the crystallization process in the neighborhood of P is influenced, leading to neutral P-defect clusters, which inhibit electrical activation. Reduced temperature ramping helps partially to activate P in implanted amorphous Ge layers. A conclusion of these results is that for high implantation doses, for which the layer is completely amorphized, the dopant activation efficiency decreases. We therefore propose to divide a high dose into multiple lower doses and activate these doses in between to prevent complete amorphization and low activation.

Acknowledgments

R.R.L acknowledges support as Research Fellow of the Research Foundation – Flanders (FWO) and support of the Belgian American Educational Foundation (BAEF). Some of the authors (R.R. Lieten, J.W Beeman, and E.E. Haller) acknowledge support by the Director, Office of Science, Office of Basic Energy Sciences, Materials Sciences and Engineering Division, of the U.S. DOE under Contract No. DE-AC02-05CH11231.

References

1. V. I. Fistul, M. I. Iglitsyn, and E. M. Omelyanovskii, *Sov. Phys. Solid State*, **4**, 784 (1962).
2. R. F. Potter, *Handbook of Optical Constants of Solids II.* (Academic, New York, 1985), p.465.
3. E. Simoen, A. Satta, A. D'Amore, T. Janssens, T. Clarysse, K. Martens, B. De Jaeger, A. Benedetti, I. Hoflijk, B. Brijs, M. Meuris, and W. Vandervorst, *Materials Science in Semiconductor Processing*, **9**, 634 (2006).
4. C. H. Poon, L. S. Tan, B. J. Cho, and A. Y. Du, *J. Electrochem. Soc.*, **152**, G895 (2005).
5. S. C. Jain, W. Schoenmaker, R. Linday, P. A. Stolk, S. Decoutere, M. Willander, and H. E. Maes, *J. Appl. Phys.*, **91**, 8919 (2002).
6. S. Mirabella, D. De Salvador, E. Napolitani, E. Bruno, and F. Priolo, *J. Appl. Phys.*, **113**, 031101 (2013).
7. R. R. Lieten, S. Degroote, M. Leys, N. E. Posthuma, and G. Borghs, *Appl. Phys. Lett.*, **94**, 112113 (2009).
8. J. Vanhellemont and E. Simoen, *Materials Science in Semiconductor Processing*, **15**, 642 (2012).
9. www.srim.org
10. E. G. Seebauer and K. W. Noh, *Materials Science and Engineering R*, **70**, 151 (2010).
11. G. G. Devyatykh, V. K. Vasil'ev, V. A. Gavva, A. V. Gusev, Yu. A. Danilov, E. S. Zharkov, and G. A. Maksimov, *Inorganic Mat.*, **32**, 1258 (1996).
12. M. Posselt, B. Schmidt, W. Anwand, R. Grötzschel, V. Heera, A. Mücklich, C. Wündisch, W. Skorupa, H. Hortenbach, S. Gennaro, M. Bersani, D. Giubertoni, A. Möller, and H. Bracht, *J. Vac. Sci. Technol. B*, **26**, 430 (2008).
13. A. Satta, E. Simoen, R. Duffy, T. Janssens, T. Clarysse, A. Benedetti, M. Meuris, and W. Vandervorst, *Appl. Phys. Lett.*, **88**, 162118 (2006).
14. E. Simoen and J. Vanhellemont, *J. Appl. Phys.*, **106**, 103516 (2009).
15. Vl. Kolkovsky, S. Klemm, and J. Weber, *Semicond. Sci. Technol.*, **27**, 125005 (2012).
16. C. Claeys and E. Simoen, *Germanium-Based Technologies: From Materials to Devices*, 1st ed. (Elsevier, New York, 2007).
17. R. R. Lieten, S. Degroote, F. Clemente, M. Leys, and G. Borghs, *Appl. Phys. Lett.*, **96**, 052109 (2010).
18. H. Haesslein, R. Sielemann, and C. Zistl, *Phys. Rev. Lett.*, **80**, 2626 (1998).
19. J. S. Williams and R. G. Elliman, *Phys. Rev. Lett.*, **51**, 1069 (1983).
20. B. C. Johnson, P. Gortmaker, and J. C. McCallum, *Phys. Rev. B*, **77**, 214109 (2008).
21. B. C. Johnson, T. Ohshima, and J. C. McCallum, *J. Appl. Phys.*, **111**, 034906 (2012).
22. S. Brotzmann, H. Bracht, J. Lundsgaard Hansen, A. Nylandsted Larsen, E. E. Haller, J. S. Christensen, and P. Werner, *Phys. Rev. B*, **77**, 235207 (2008).
23. J. Kim, S. W. Bedell, and D. K. Sadana, *Appl. Phys. Lett.*, **101**, 112107 (2012).